MIT Libraries | DSpace@MIT

MIT Open Access Articles

Progress Toward Diamond Power Field-Effect Transistors

The MIT Faculty has made this article openly available. ***Please share*** how this access benefits you. Your story matters.

Citation: Geis, Michael W., Wade, Travis C., Wuorio, Charles H., Fedynyshyn, Theodore H., Duncan, Bradley et al. 2018. "Progress Toward Diamond Power Field-Effect Transistors." physica status solidi (a), 215 (22).

As Published: http://dx.doi.org/10.1002/pssa.201800681

Publisher: Wiley

Persistent URL: https://hdl.handle.net/1721.1/140893

Version: Author's final manuscript: final author's manuscript post peer review, without publisher's formatting or copy editing

Terms of Use: Article is made available in accordance with the publisher's policy and may be subject to US copyright law. Please refer to the publisher's site for terms of use.

Massachusetts Institute of Technology

Check for updates

Article Type: Feature Article
TOC-Keyword: Diamond Field-Effect Transistors

Progress Toward Diamond Power Field-Effect Transistors

M. W. Geis*, T. C. Wade*, C. H. Wuorio, T. H. Fedynyshyn, B. Duncan, M. E. Plaut, J. O. Varghese, S. M. Warnock, S. A. Vitale and M. A. Hollis

Massachusetts Institute of Technology, Lincoln Laboratory, Advanced Technology Division
244 Wood St., Lexington, MA
*Corresponding Authors: Michael Geis, MIT Lincoln Laboratory, 244 Wood St, Lexington, MA
Travis Wade, Plasmability LLC, 4715 Steiner Ranch Blvd, Austin, TX

Author Manuscript

This is the author manuscript accepted for publication and has undergone full peer review but has not been through the copyediting, typesetting, pagination and proofreading process, which may lead to differences between this version and the Version of Record. Please cite this article as doi: 10.1002/pssa.201800681

This article is protected by copyright. All rights reserved

Abstract

Diamond's properties (highest thermal conductivity, high hole & electron mobilities, & high electric breakdown field) predict that diamond field-effect transistors (FETs) would have superior high-power high-frequency performance over FETs formed in other semiconductors. The development of diamond FETs was limited by a lack of quality substrates & the high ionization energy of the primary dopant, boron (B). This high ionization energy results in a resistance too high for FETs.

Fortunately, recent developments are addressing these shortcomings. Single-crystal diamond substrates ≈4 inches are demonstrated. Further, two approaches address the dopant issue. When the surface of diamond is terminated in H, a surface p-type conductive layer forms. FETs made using this layer demonstrate competitive high-frequency performance, though manufacturability of this type of device has yet to be worked out.

The second solution to doping uses delta doping by B. A thin < 2-nm layer doped with B at > 10^{20} cm^{-3} is sandwiched within undoped diamond. This structure mitigates B's high ionization energy by producing an acceptor subband with ~ 100% of the B is ionized. Recent reports of delta-doped diamond have channel resistances suitable for device applications.

This article will review the state of the art for FET and substrate development.

Author Manuscript

1. Introduction

1.1 Comparison to other semiconductors Diamond has a combination of electrical and thermal properties that make it unique among all the semiconductors for transistor applications. It has the highest room-temperature thermal conductivity, high hole and electron mobilities, high electric breakdown field, and a large bandgap (5.47 eV).[1] These properties are summarized in **Table 1**. Each of these properties contribute to desirable transistor properties. Thermal conductivity relates to the power dissipation a transistor can safely handle.

Table 1. Summary of electrical and thermal properties of commonly used and future semiconductors. The higher thermal conductivities for diamond and cubic BN are for isotopically pure crystals. The last row indicates the semiconductor maturity, pink being less mature. [1]

Parameter	Diamond	c-BN	β-Ga_2O_3	AlN	GaN	SiC	GaAs	Si
$\sigma_{thermal}$ (W/m•K)	2,290 - 3,450	940 - 2,145	11 - 27	319	≤ 253	370	55	145
e^- mobility (cm^2/V•s)	4,500	825	180	426	2,260	900	8,500	1,450
hole mobility (cm^2/V•s)	3,800	500	--	--	24	120	400	480
$E_{breakdown}$ (MV/cm)	~13.0	~17.5	~10.3	~15.4	~4.9	~3.0	~0.4	~0.3
v_{sat} (10^7 cm/s)	2.3 (e^-) 1.4 (h^+)	--	1.1	1.3	1.4	2.0	1.0	1.0
Rel. permittivity	5.7	7.1	10.0	9.8	10.4	9.7	12.9	11.8
Maturity								

This article is protected by copyright. All rights reserved

Desirable properties alone don't convey their relative importance. For this reason, researchers have developed a variety of figures of merit or weighted factors to allow materials to be compared directly, usually for a particular application or design criteria. The Huang chip area criteria, $HCA = \epsilon\sqrt{\mu}E_C^2$, is used to compare the size of transistors with similar properties. The larger the value, the smaller the transistor can be with the same power-handling properties.[2] The minimum power loss of a switching transistor is inversely proportional to the Huang switching criteria = $\sqrt{\mu}\,E_C$.[2] Baliga's figure of merit = $\epsilon\mu E_C^3$, which is applicable for low-frequency power applications, compares the semiconductors' power switching properties, assuming power is only dissipated during the "on" state of the transistor.[3] For high frequency applications where the period of oscillation approaches the switching time of the transistor, the Johnson figure of merit = $v_{SAT}E_C/2\pi$ is used to compare the voltage-frequency product of a transistor.[2-4] Finally, due to the omission of thermal conductivity from any of the listed figures of merit and the established fact that the performance of present-day transistors is frequently limited by thermal effects, we present thermal conductivity alongside these figures of merit. **Figure 1** summarizes the comparison of several semiconductors for these five figures of merit. If the intrinsic properties of diamond can be fully realized, the Johnson figure of merit, a metric favored by the authors, predicts diamond devices with performance triple that of as-yet-unrealized ideal GaN. The material properties of diamond plainly justify its development as a semiconductor.

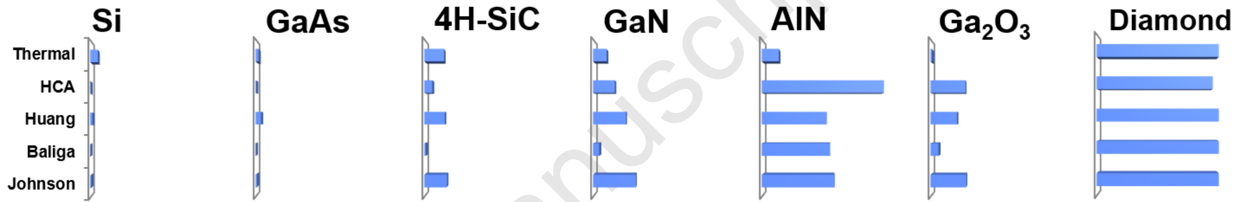

Figure 1. Bar chart showing a comparison of semiconductors using several figures of merit criteria. <qry> author: Were the figures 1—12, 14, 15, 20 and 21 taken from other publications? <qry>

1.2 Difficulty in Creating Charge Carriers in Diamond Development of diamond as a semiconductor for field effect transistors (FETs) and radio frequency (RF) devices has been limited by a lack of diamond substrates and effective dopants, the latter having high ionization energies (B @ 0.36 eV, P @ ~0.57 eV, and N @ 1.7 eV).[1,5] These high ionization energies result in room-temperature charge-carrier densities that are orders of magnitude below dopant concentration. Charge carriers (holes) at density p, generated by a dopant, density N_A, at temperature T, and ionization energy E_A are related by **Equation 1**.[6]

$$\frac{p(p+N_D)}{N_A - N_D - p} = \left(\frac{2\pi m^* kT}{h^2}\right)^{3/2} exp\left(-E_A/_{kT}\right) \qquad \textbf{Equation 1}$$

Where m^* is the reduced mass of a hole, k is Boltzmann's constant, h is Plank's constant, and N_D is the density of hole traps and donors (usually a small concentration of nitrogen or phosphorus present in the diamond). The hole density as a function of dopant density is shown by **Figure 2**.

Author Manuscript

This article is protected by copyright. All rights reserved

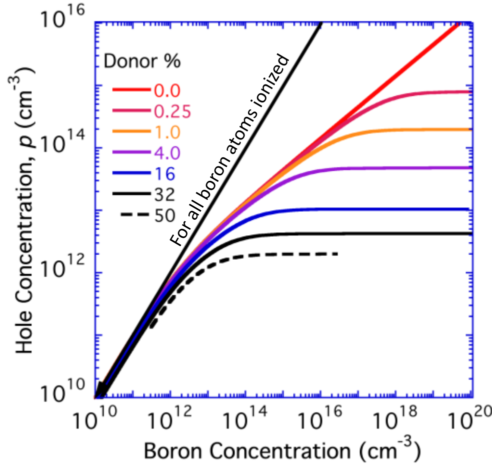

Figure 2. Hole concentration at 298 K for several donor % concentrations as a function of boron doping. The donors can be either nitrogen or phosphorus and trap the charge carriers, removing them from the valence band and making the diamond more resistive. A commonly used carrier density for transistors, 10^{16} cm^{-3}, requires >10^{19} boron concentration. If even a small fraction of nitrogen donors are incorporated into the diamond at 0.25% of the boron concentration, then the carrier density can never exceed 10^{15} cm^{-3} for any boron doping level. At doping densities >10^{19} cm^{-3} the boron atoms form a sub-band and eq. 1 is no longer applicable.[7]

From **Equation 1** it can be seen that $p \propto exp\left({-E_A}/{2kT}\right)$ if $N_A >> p$, which is nearly always the case at room temperature and $N_D=0$. This means the carrier density increases by $exp\left({-0.18\ eV}/{kT}\right)$ or ~2-fold for every 30 °C. However, if donors are present in the diamond and $N_D >> p$ then $p \propto exp\left({-0.36\ eV}/{kT}\right)$ and carrier density increases by ~2-fold for every 15 °C. To the authors' knowledge, for boron levels < 10^{19} cm^{-3}, reported carrier density as a function of temperature increases by ~2 for every 15 °C, exhibiting a thermal activation energy of 0.36 eV instead of 0.18 eV, indicating the difficulty of removing donors in boron doped diamond. These low carrier densities make boron doped diamond too resistive to compete with other semiconductor transistors at room temperature. Diamond n-type dopants, like phosphorus and nitrogen, have even higher activation energies and resistances.

2. Conductive Diamond for FETs

This article discusses two solutions to the low carrier densities and the high resistance problem. The first exploits the unusual properties of a diamond surface that is terminated with hydrogen. In this case, a surface dipole is generated that lowers the energy required to pull an electron out of diamond's valence band from 7.2 eV to 4.2 eV.[8] This enables electrons can leave the diamond and be captured by materials on the surface having higher binding energies than the H-terminated diamond. A resulting p-type conductive layer of holes forms just under the diamond surface that has sufficient conductivity to be used for competitive FETs. This process is referred to as surface transfer doping or activation, where the carriers are in the semiconductor and the dopants (electron-capture species) exist in an adjacent overcoating material matrix. Adsorbed gases on the diamond surface, H_2O with pH < 6 from atmospheric impurities,[9] NO_2,[10-13] O_3,[11] and solid metal oxides $(NH_4)_3Ce(NO_3)_6$,[13] Al_2O_3,[14,15] WO_3, MoO_3, and V_2O_5[16-18] all have demonstrated the ability to generate a diamond-surface-conductive layer. FETs fabricated using a combination of adsorbed NO_2 with Al_2O_3[19] and Al_2O_3 with poly-tetra-fluoro-ethylene[20] have exhibited impressive device properties with current densities from 1.2 to 1.3 A/mm. An example is shown in **Figure 3**. Al_2O_3 overcoated diamond devices have demonstrated a wide operational temperature range, -263 (10 K) to 400 °C,[21] high voltage operation > 1 kV,[22] unity-

This article is protected by copyright. All rights reserved

current-gain frequency, f_T , of 70 GHz,[23] and maximum frequency of oscillation, f_{max}, of 120 GHz.[24,25] The high voltage operation and inherent high thermal conductivity, ~ 20 times that of Si, demonstrates the feasibility of a diamond FET superior to those formed in other semiconductors.

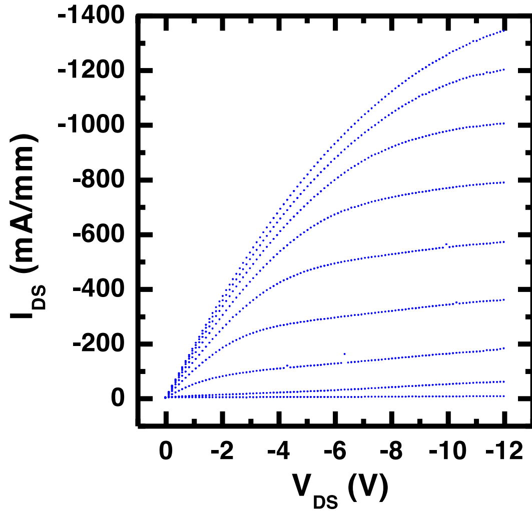

Figure 3. Drain current I_{DS} as a function of drain-source voltage V_{DS} of a 0.4-μm-gate-length diamond FET with a NO_2 - Al_2O_3 activation layer. The gate-source voltage was varied from V_{GS} = +11 to -5 V in ΔV_{GS} = -2 V steps. The device was fabricated on a polycrystalline diamond substrate.[19] Reprinted with permission from Jpn. J Appl. Phys., K. Hirama, H. Sato, Y. Harada, H. Yamamoto, M. Kasu, Diamond Field-Effect Transistors with 1.3 A/mm Drain Current Density by Al_2O_3 Passivation Layer, 51 (2012) 090112.

A second potential solution to the problem of diamond charge carriers uses boron in delta-doped layers. A very thin layer, < 2 nm, with sharp, well-defined boundaries of heavily boron-doped diamond, > 10^{20} cm^{-3}, is grown epitaxially within an undoped diamond layer. The wave functions of holes in the boron-doped layer extend into the nearby high-mobility intrinsic layer,[26,27] thus increasing carrier mobility. Further, in such highly doped diamond, a dopant subband forms which raises the activation of the boron to nearly 100%. For comparison, if the boron was uniformly distributed, < 1% of the boron atoms would contribute holes, making the material too resistive through both low carrier density and degraded mobility. There are numerous reports on delta-doped diamond, but the device quality of these layers has been disappointing until recently.[28-32]

Author Manuscript

2.1 Generating diamond surface conduction As described above, when the H-terminated diamond surface is overcoated with a material that has a higher electron-binding energy, electrons leave the diamond and attach themselves to the overcoating material, thereby producing a conductive layer of holes in the diamond surface. Work with several of these materials—NO_2, transition metal oxides, and Al_2O_3—is discussed below.

2.1.1 Transfer Doping with NO_2 The presence of NO_2 in concentrations as small as 6 ppb makes H-terminated diamond conductive.[10,11] At higher NO_2 concentrations, the lowest reported surface resistance of ~700 Ω sq^{-1} [33] and highest reported transistor drain current of

This article is protected by copyright. All rights reserved

1.35 A mm^{-1}[19] were achieved. Initially, it was believed that adsorbed NO_2 was taking electrons from the diamond, forming NO_2^-.[34,35] However, no NO_2^- could be detected on the diamond surface, but instead NO_3^- was found at concentrations approximately equal to the positive charge density in the diamond.[12] Given the difficulty of accurately characterizing a sub-monolayer of adsorbed material, these results were obtained from the surface chemistry of diamond powder, < 250 nm in diameter, where the surface area is increased by ~ 10^4 over a diamond plate. This increase in surface area allowed for infrared transmission to detect the surface chemistry. **Figure 4** shows the diamond powder during H-termination, and the Fourier transform infrared spectroscopy, FTIR, measurements of diamond powder before and after H-termination are displayed in **Figure 5**. Details of H termination and FTIR procedures are presented in reference [12]. Before H-termination, the infrared absorption peaks are consistent with the powder terminated with O and OH groups. After H-termination, the O chemistry is gone and replaced with absorption peaks at 2920-2927 and 2834-2840 cm^{-1}, which are consistent with C-H absorption on the (100) and (111) diamond crystal planes.

Figure 4. Diamond powder during H-termination in a hydrogen plasma at ~ 60 Torr of H_2. The powder is initially heated by the plasma to ~1000°C for 10 min to degas the powder and then H terminated for 60 min at ~800°C.[12]

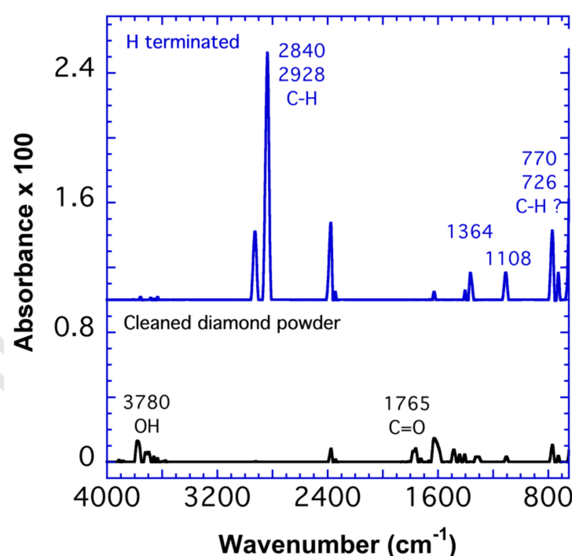

Figure 5. Fourier transform infrared absorption, FTIR, of diamond powder before ("cleaned diamond powder") and after H-termination.[12]

After H -termination, the diamond powder was exposed to NO_2[12] whereupon the FTIR absorption changes dramatically. **Figure 6** shows the FTIR absorption after H-termination as shown in **Figure 5** for comparison with the same powder after NO_2 exposure. The signature for C-H is suppressed by a factor of ~5, absorption consistent with OH appears, and most importantly there is no evidence of NO_2^- at 2557 and 1270 cm^{-1}. Instead, a very strong absorption appears at 1382 cm^{-1}, which is consistent with NO_3^-. At atmospheric pressure and room temperature, NO_2 is in equilibrium with its dimer, N_2O_4. We speculate that the dimer reacts to remove an electron from the diamond and thus dissociates into NO and NO_3^- by the reaction shown in **Figure 7**.

This article is protected by copyright. All rights reserved

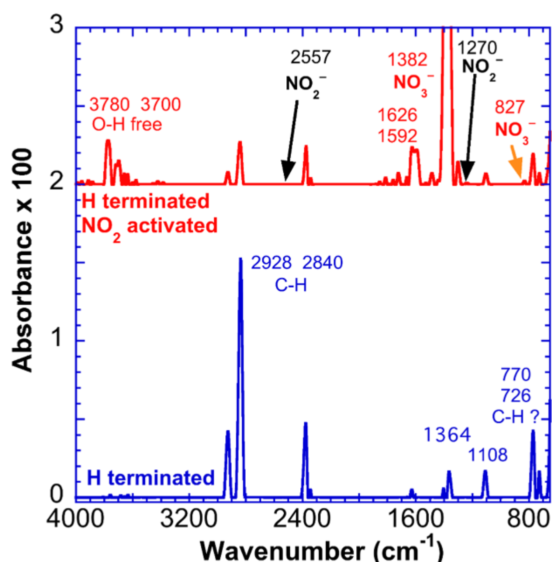

Figure 6. FTIR of H-terminated diamond powder before and after NO_2 exposure. No absorption for NO_2^- at 2557 and 1270 cm^{-1} was measured. The absorption peak corresponding to NO_3^- at 1382 cm^{-1} is off scale[12].

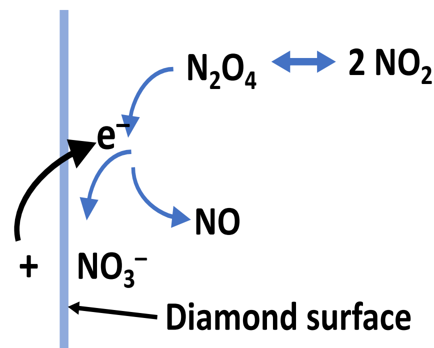

Figure 7. Possible reaction of NO_2 with H-terminated diamond to form a negative ion on the diamond surface and a positive carrier in the diamond.

Although absorption at 1382 cm^{-1} is consistent with NO_3^-, further evidence is desirable to rule out that another carbon complex could be responsible for this absorption or that additional absorption peaks could be hidden at 1382 cm^{-1}. To unequivocally determine that the absorption at 1382 cm^{-1} is only from NO_3^-, isotopically enriched $N^{15}O_2$ was used to replace the $N^{14}O_2$ used in the experiments. **Figure 8** shows the absorption of two H-terminated diamond powders, one exposed to $N^{14}O_2$ and the other exposed to $N^{15}O_2$. The shift in the resulting absorption peak from 1382 to 1352 cm^{-1} not only indicates that we are actually forming NO_3^- on the diamond surface, but that there is no hidden chemistry associated with absorption in the region of 1382 cm^{-1}.

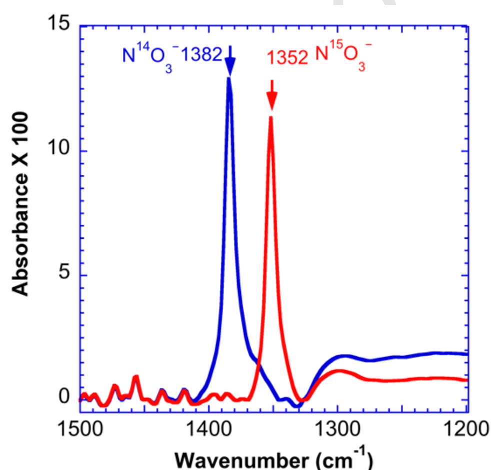

\

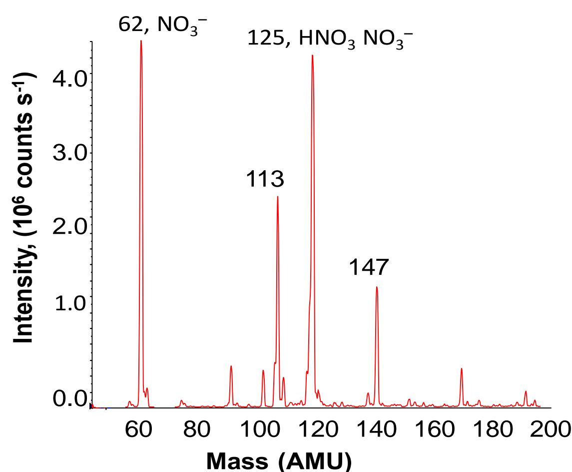

This article is protected by copyright. All rights reserved

Figure 8. FTIR absorption of two H-terminated diamond powders, one exposed to $N^{14}O_2$ in blue and the other exposed to $N^{15}O_2$ in red.

Figure 9. Electrospray spectrometer scan of water used to wash nitrate from the diamond powder. These results corroborated other measurements of surface concentration of NO_3^- on the diamond powder.[12]

The concentration of NO_3^- was additionally measured by washing the NO_2-exposed powder with water. NO_3^- dissolved in the water and its concentration was measured both by electrospray spectrometer, **Figure 9**, and colorimetric techniques. Using the surface area of the diamond powder, 47.3 cm^2 mg^{-1}, determined by the (Brunauer, Emmett and Teller) BET technique,[36] the surface density of NO_3^- as determined by electrospray and colorimetry was 6.3×10^{13} and 8.2×10^{13} cm^{-2}, respectively. Van der Pauw and Hall measurements of the carrier density for single-crystal H-terminated and NO_2-exposed (100) diamond plates yield 3×10^{13} - 9×10^{13} cm^{-2}. This agreement between surface density of NO_3^- and carrier density is well within the uncertainty of the measured NO_3^- .

Conductive H-terminated diamond is commonly modeled by transfer doping where an electronegative overcoating pulls electrons out of the diamond, generating hole carriers. The model assumes that there are no chemical reactions between the H-terminated diamond and the overcoating material. When NO_2 is applied to H-terminated diamond and reacts with the diamond surface to form NO_3^-, the concentration of hydrogen bonded to the diamond surface is reduced by 2 to 10 times as measured by the FTIR signature of the C–H bond. Additionally, the O–H FTIR signature of the diamond-O-H structure appears, as shown in **Figure 6**. This indicates that either the H atoms are removed and oxidized during transfer doping with NO_2 or that the FTIR C–H signature is suppressed by the presence of NO_3^-. One speculation is that the NO_2 reacts with some of the less strongly bonded H on the surface by **Equation 2**.[12]

$$\bullet NO_2 + C\text{-}H \rightarrow HNO_2 + C\bullet \qquad \textbf{Equation 2}$$

Where the H is removed, additional chemical reactions would occur forming C-O-H. If this is the case then the surface conductance would vary with the local chemistry over a submicron scale potentially reducing the hole mobility. In spite of the potential for locally non-uniform conduction, NO_2 activated diamond is one of the lowest resistive surfaces to date, ~700 Ω sq^{-1}.[33] Only O_3 of the transfer doping gases has a lower resistance.[11] Ley et al. reported that O_3 chemically reacts with the H-terminated diamond surface and the reaction enhances the transfer doping conductance.[37] He speculated a small fraction of the diamond surface, ~1%, is oxidized by O_3 forming either ether groups, C–O–C, or alcohols, C–O–H. The other diamond transfer doping materials $(NH_4)_3Ce(NO_3)_6$, MoO_3, WO_3, and V_2O_5, are known for their oxidizing properties and may have similar chemical reactions. The simple models of transfer doping may require some additional modifications.

As discussed above, NO_2 on H-terminated diamond generates one of the lowest surface resistances of any diamond treatment and the highest reported drain current. We also observe that the resistance increases with time making it unusable for devices. **Figure 10** shows the resistance of single crystal (100) H-terminated diamond in air, after NO_2 exposure, and NO_2 exposed and kept in dry N_2. H-terminated diamond will become conductive in air by exposure to the O_3 and/or NO_2 in the atmosphere. However, this conductance is temporary and variable.

This article is protected by copyright. All rights reserved

Author Manuscript

In dry N_2, the resistance, at the scale in **Figure 10,** appears stable over days but this is in part due to the anticorrelation between the carrier density and mobility as seen in **Figure 11**. **Figure 11** also shows that the density logarithmically decreases in time, and the lithographic process used to make FETs is observed to increase the resistance (data not shown). Because of the instability of NO_2-enhanced conductivity, other approaches are being pursued, including atomic layer deposition (ALD) of Al_2O_3 and transition metal oxides like MoO_3, WO_3, and V_2O_5, which will be discussed next.

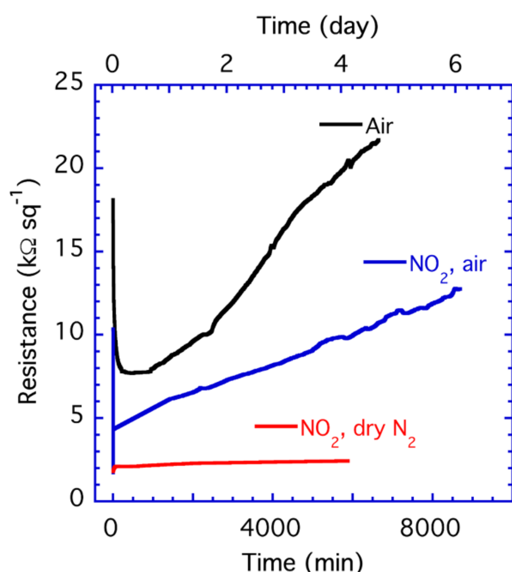

Figure 10. Resistance of single crystal (100) H-terminated diamond as a function of time for three treatments: In air, NO_2-exposed then kept in air, and NO_2-exposed then kept in dry N_2.

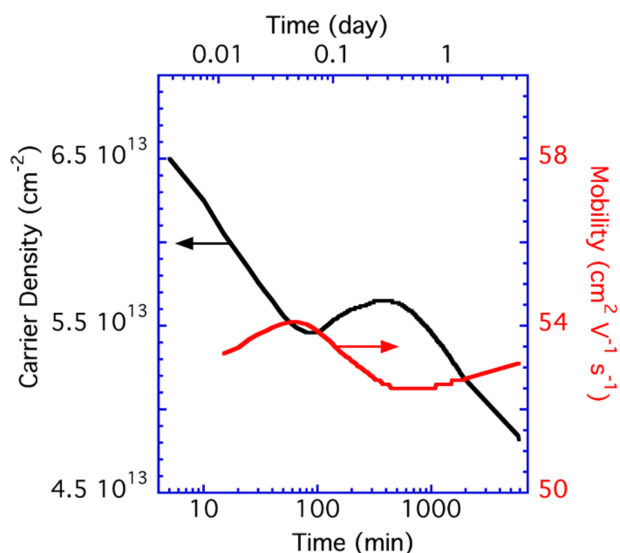

Figure 11. Carrier density and Hall mobility of the sample exposed to NO_2 and kept in dry N_2 from **Figure 10** plotted as a log function of time. Note: The carrier densities were only estimated from the surface resistance and the Hall mobility. The drift mobility, which can differ from the Hall mobility by the Hall correction factor,[38] is required to accurately calculate the carrier density. The Hall correction factor is due to the nonsphericity of the Fermi surface and has not been applied as it is unknown for the surface of diamond.

2.1.2 Transition Metal and Aluminum Oxides Kueck [14] first reported the use of ALD of Al_2O_3 to stabilize diamond's surface conductance. Metal-insulator field-effect transistors, MISFETs, made with this coating were stable in time over a wide range of temperatures and were reasonably stable under high voltage operation.[21.22] However, the high surface resistance from 8 to 12 kΩ sq^{-1} for (100) oriented diamond substrates limits the drain current[39]. Looking for a coating that would both stabilize the diamond surface and generate resistances < 5 kΩ sq^{-1}, the transition metal oxides WO_3, MoO_3, V_2O_5, Nb_2O_3, and ReO_3 were considered. Some of these oxides had been previously used with organic solar cells because of their high electron work function.[40] As the work function of these oxides increases in **Figure 12**, the energy difference (activation energy) between the diamond valence band and the oxide's conduction band increases. As the activation energy increases, the carrier density in the diamond would be expected to increase also, which has been demonstrated by Verona et al. [41] in **Figure 13**. These oxides are easily deposited by thermal evaporation on diamond and

This article is protected by copyright. All rights reserved
Author Manuscript

generate high sheet carrier densities approaching ~10^{14} cm^{-2} with surface resistances of 2.7 and 1.8 kΩ sq^{-1} for (100) and (111) diamond surfaces respectively.[43]

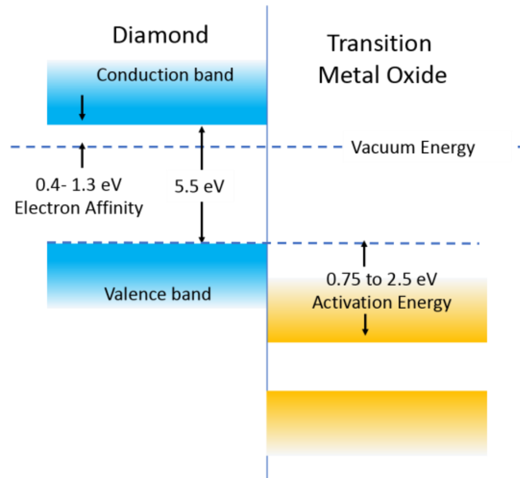

Figure 12. Band diagram of diamond and a transition metal oxide. The electron affinity of diamond varies with crystal plane and surface termination.[42]

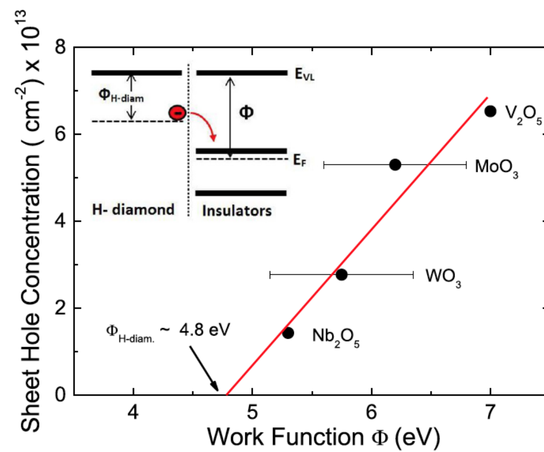

Figure 13. The sheet carrier density in the diamond increases with the increase in the energy difference between the top of diamond's valence band and the bottom of the transition metal oxide's conduction band. Reproduced with the permission.[41] Copyright 2016, American Institute of Physics.

The stability of these transition metal oxide films is superior to that of NO_2, but the level of stability found with Al_2O_3 has not yet been demonstrated by them. V_2O_5 on diamond exhibited surface conduction that varies < 10% over temperatures of -200 to 200°C in vacuum[43]. Crawford[44] found that when V_2O_5 and MoO_3 are heated in air above 100°C, a significant increase in diamond's resistance occurs and remains high after cooling. However, encapsulating the films with a spin on glass, HSQ, stabilized the diamond resistance up to 300°C.

There are also other concerns with transition-metal-oxide transfer doping. Although resistances of ~2 kΩ sq^{-1} can be obtained, the highest reported drain current is < 0.4 A mm^{-1}, whereas the use of ALD Al_2O_3 yields surface resistances of 4 to 12 kΩ sq^{-1} [39] but obtains 0.8 to 1.2 A mm^{-1}.[39,45] These transition metal oxides are themselves semiconductors with a complex range of oxidation states. Under the operating conditions of a MISFET, current may pass through these films, potentially changing their oxidation states and resulting in a material with a lower electron affinity and a corresponding increase in surface resistance. Future efforts will elucidate the cause of the lower drain currents of transition metal oxide MISFETs.

2.1.3 ALD Aluminum Oxide Another overcoating material, Al_2O_3, has resulted in low surface resistance as reported above. The classic transfer-doping model where the conduction band of the coating material is below diamond's valence band does not apply in this case, as the conduction band of Al_2O_3 is ~3 eV above the valence band of diamond.[46] However, Al_2O_3 can contain electron traps below diamond's valence band.[46] We speculate that these traps are responsible for the enhanced conduction with ALD Al_2O_3. By varing the ALD parameters and

This article is protected by copyright. All rights reserved

controlling impurities in the ALD deposition, we have obtained surface resistances between 1.5 and 2.5 kΩ sq^{-1}. **Figure 14** compares the resistance of three H-terminated diamonds aged in air over many days—after being activated by air, NO_2, and ALD Al_2O_3, respectively. Overcoating with Al_2O_3 adds stability to the carrier density as shown in **Figure 15** compared to NO_2-activated diamond in dry N_2 in **Figure 11**. However, the stability of these ALD Al_2O_3 films has not been evaluated under actual MISFET operation.

Reproducibility and stability of FETs with high drain currents ≥ 1 A mm^{-1} has yet to be demonstrated. Thus, much of the remaining research in diamond is directed to developing a stabilizing layer on diamond that enables reproducible high-current, high-voltage FETs with practical lifetimes.

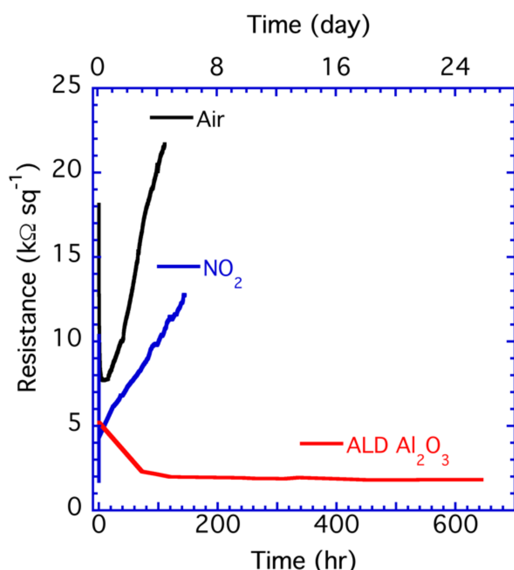

Figure 14. Comparison of surface resistance of three H-terminated diamonds aged in air. One was activated by air, one by NO_2 as shown in **Figure 10**, and one by ALD Al_2O_3.

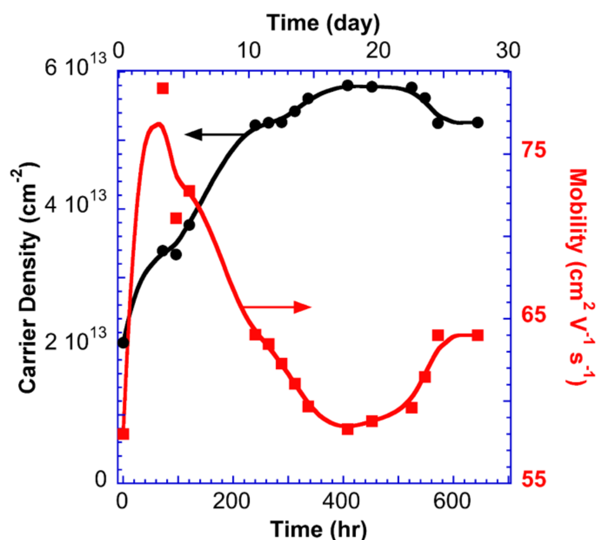

Figure 15. Carrier density and Hall mobility of the ALD Al_2O_3 sample from **Figure 14** plotted as a function of time. Note: The carrier densities were only estimated from the surface resistance and the Hall mobility. The drift mobility, which can differ from the Hall mobility,[38] is required to accurately calculate the carrier density.

2.2 Boron Delta Doping The second potential source of conductive diamond for FETs, delta doping, is obtained by embedding a very thin layer, ≤ 2 nm (< 6 diamond unit cells), of high boron doping, > 10^{20} cm^{-3}, into an otherwise undoped diamond. Modeling has predicted for these thin layers that the carriers are quantum confined[26,27] and Kohn et al.[47] have predicted that RF FETs made with the diamond structure shown in **Figure 16** would have current capacity of 2.5 A mm^{-1} and RF power generation from 34 W mm^{-1} to 75 W mm^{-1}, depending on the gate structure and the desired frequency of operation. These remarkable properties are the result of the hole wave function being larger than the thickness of the delta layer which allows a portion of the wave function to exist in the undoped regions of the diamond where the hole mobility can be significantly higher than for a uniformly doped material. With a material doped uniformly at < mid-10^{19} cm^{-3}, < 1% of the boron dopants would

This article is protected by copyright. All rights reserved

generate holes at room temperature whereas nearly 100% of the boron is activated in the delta-doped layer.

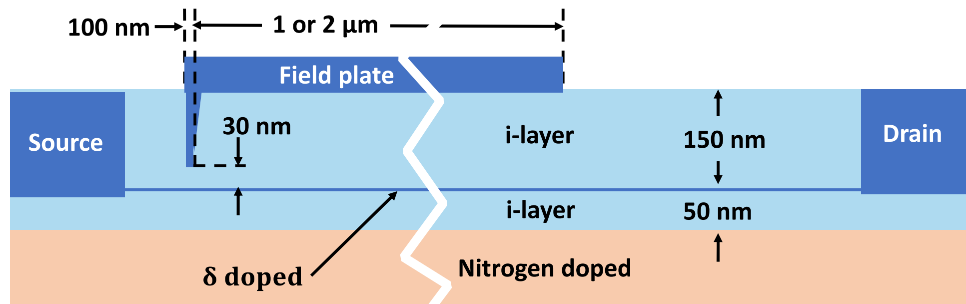

Figure 16. To-scale schematic cross section of a delta-doped p-channel FET with a recessed gate and planar field plate used for device modeling. Reproduced with permission.[47] Copyright 2005, Elsevier B.V.

The only known technique that could generate such a diamond structure is epitaxial growth with exquisite control over the starting diamond surface roughness, growth rate, impurities, and boron dopant. Several attempts to create such a structure have been reported, but electrical measurements did not show the expected low resistance and high mobilities.[28-32] Kohn[48] suggested that the poor result is due to nonuniform boron doping in the delta layer, resulting in boron clusters, which he observed in cross sectional high-resolution transmission electron microscopy, HR-TEM. Using a variable-range hole hopping model between boron clusters at the scale measured by HR-TEM, a good fit for the resistance as a function of temperature was obtained. The clustering is felt to be due to surface roughness of ≥ 1 nm created by pre-etching the diamond and growth before the boron doped layer is grown. This results in boron incorporation varing at surface steps and ridges, generating discontinues in the very thin < 2-nm delta-doped layer.

Only recently has a diamond growth system been specifically designed for delta doping using very smooth starting diamond substrates. It has shown promising initial results, detailed in works by Butler and Lobaev et al.[28,49] For the first time to these authors' knowledge resistances < 10 kΩ sq^{-1} (1.1 to 7 kΩ sq^{-1}) with mobilities from 16 to 120 $cm^2\ V^{-1}\ s^{-1}$ (approaching the predicted mobilities of 150 to 200 $cm^2\ V^{-1}\ s^{-1}$[47,48]) have been consistently obtained. Their experimental set up is similar to others. Diamonds polished to < 0.3-nm roughness with 1° miscut angle off the (100) plane (experimentally found to give the best results) were used in the experiments. After plasma etching 4-5 µm of the diamond surface to remove polishing damage, a growth rate of 30 to 90 nm hr^{-1} was established. B_2H_6 at 0.1% level was introduced into the growth chamber to obtain the doped regions. With a residual gas residence time of 5 seconds, this system generated a concentration of boron in the unintentionally doped regions of less than 10^{17} cm^{-3}, which is believed to be adequate for high mobility. H_2S was added to the gas flow to getter residual boron during the growth of undoped diamond. Secondary ion mass spectroscopy, SIMS, and capacitance-voltage measurement of diodes cannot resolve the doping density of the delta layer, but estimates are ~$4x10^{20}$ cm^{-3} boron in a 1 nm thick layer. The fabrication of FETs on these films will determine their potential for high power RF devices.

This article is protected by copyright. All rights reserved

3. Large-Area Diamond Substrates

The full realization of diamond's device performance heralded by the figures of merit in **Figure 1** is also limited by the lack of large-area diamond substrates with device research limited to diamond substrates a few to 10 millimeters on a side. Naturally sourced crystals will not satisfy chemical purity nor geometric requirements and have significant shortcomings in reproducibility. High pressure, high temperature (HPHT) material is in ready supply in small, blocky shapes and serves the diamond tool-cutting and gemstone markets very well but the crystals are not large enough for good electronic development. The desire is strong for wafer-scale diamond, and multiple approaches are under simultaneous development worldwide.

3.1 Polycrystalline Wafers Efforts are underway to determine which applications might be served by the far more immediately scalable polycrystalline diamond wafers. The highest FET current densities yet reported have been fabricated on polycrystalline diamond.[50,19] This is in part because the (110) oriented diamond, common to polycrystalline diamond substrates, has a higher electrical surface conductance than (100) oriented substrates when activated with similar technologies.[39,50] Since the grain boundaries are not shorts and the FETs' drain to source distances, 0.5 to 10 μm, can be smaller than the crystals in the substrate, there are not significant compromises using polycrystalline films for small FETs for research work. Large area (110) oriented polycrystalline substrates are comparatively easy to grow or obtain. CVD-grown polycrystalline diamond is commercially available from a variety of sources up to 2 and as large as 6 inches from a few select providers. Hot filament (HF) growth tools have demonstrated scalable, cost-effective coating capability and can produce near-optical-quality microcrystalline material. An example of a HF system is shown in **Figure 17**. To date, neither HPHT diamond synthesis nor HF techniques have shown great progress towards producing wafer-scale monocrystalline diamond.

Author Manuscript

This article is protected by copyright. All rights reserved

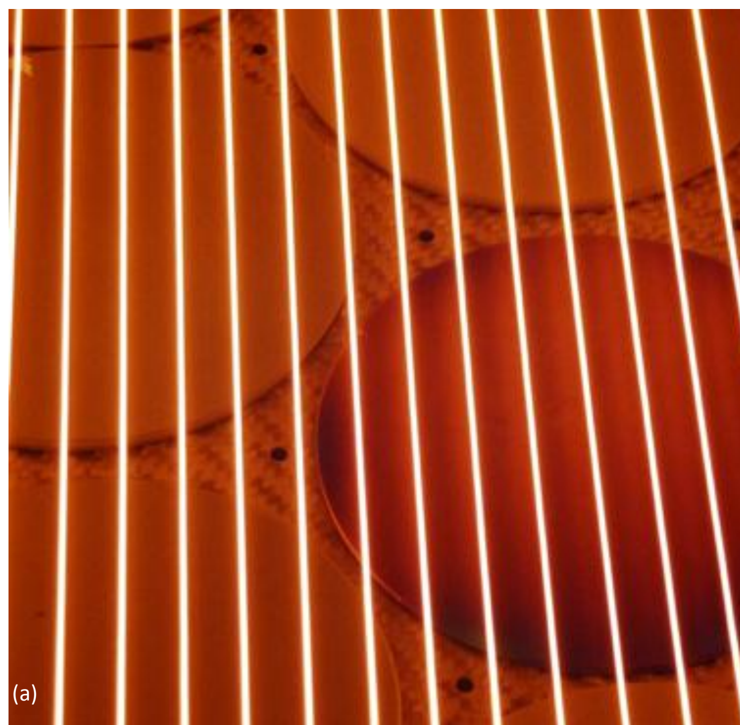

Figure 17. (a) Top view and (b) side view of silicon wafers being coated with a polycrystalline diamond film in a hot filament CVD reactor. Deposition areas as large as 400x1180 mm (0.5m^2) have been coated with this technology. Photo courtesy of Neocoat SA.[51] <qry> Author: did you ask for permission to use this images?<qry>

3.2 Homoepitaxial Single-Crystal Diamond Growth A high atomic hydrogen flux is generally viewed as essential for CVD deposition of high-quality diamond.[52,53] As a result, plasma CVD has been shown to be a promising method to grow high-quality material, but has its own challenges and limitations. Chief among these are vacuum-chamber constraints, uniformity, scalability, and the thermal engineering challenges associated with a high-energy plasma. There is only one plasma CVD method that does not require a vacuum chamber and has demonstrated scalability, the DC arc jet, but the material quality is low and the output is primarily used in mechanical applications where the optical and electrical properties of the diamond are unimportant.[54]

The challenges of homoepitaxial growth of diamond in plasma CVD have been largely mitigated, and there are many companies that have sprung into existence to leverage this

This article is protected by copyright. All rights reserved

knowledge. In general, homoepitaxy does not yield a useful surface larger than the initial substrate. However, some variations on homoepitaxy can increase the substrate size. Homoepitaxial growth on carefully selected rather small single crystals with minimum dislocation densities can be performed in such a way that the available area is increased step by step while the dislocation density is kept low, as depicted in **Figure 18**.[55] By such an approach, 4H-SiC has progressively been scaled over 20 years starting from small platelets to a 6-inch wafer size.[56]

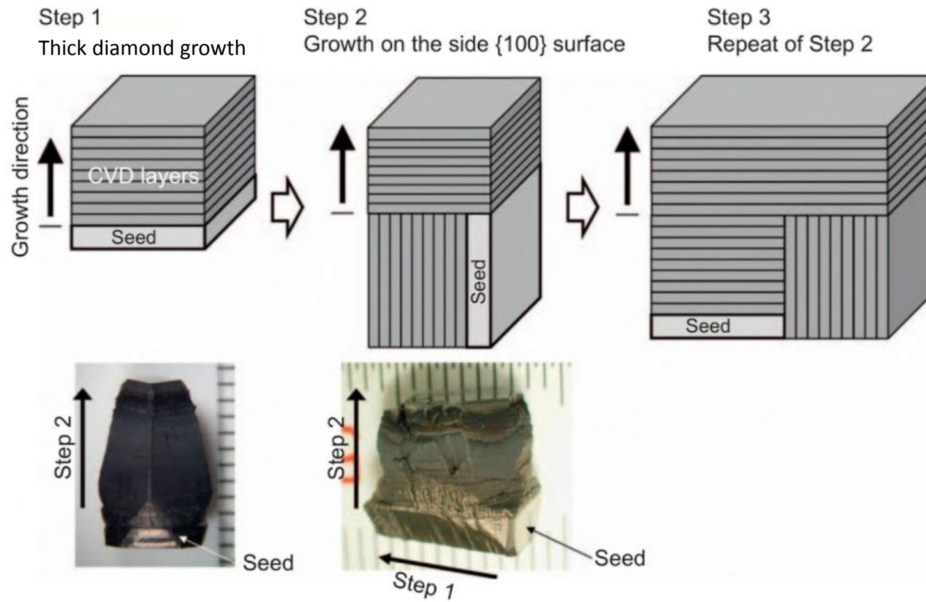

Figure 18. An example of homoepitaxial growth on different facets to increase the size of the starting substrate. Reproduced with permission.[55] Copyright 2006, Elsevier B.V.

3.3. Mosaic Tiling The idea of tiling diamond substrates together and growing epitaxy to "glue" them together and make a cohesive epi-layer as illustrated in **Figure 19** has seen decades of development. Despite the challenges of precisely aligning the substrates, the approach has seen some successes. Boundaries at crystal joints continue to contain a higher concentration of defects (and often impurities). Time will tell if these defects can be reduced to the point that the optical and electrical properties become unimpeded.

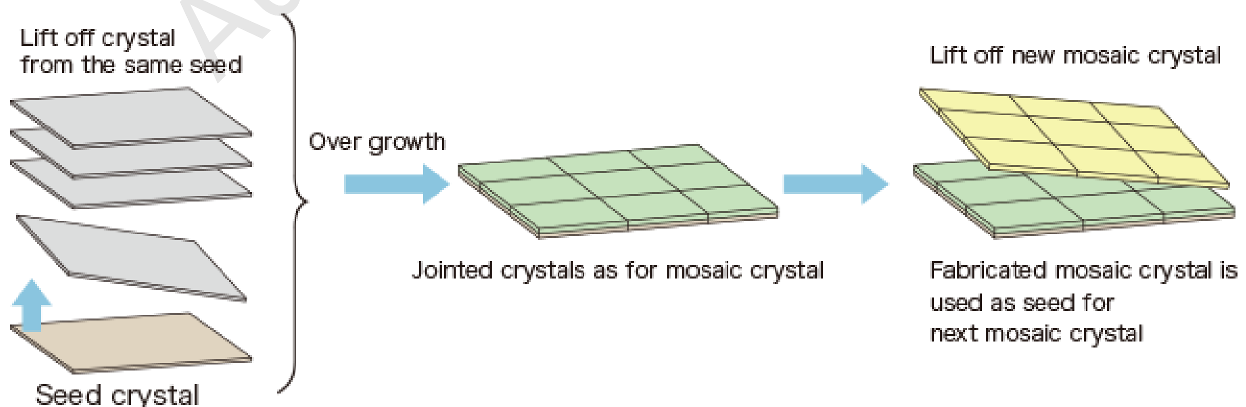

This article is protected by copyright. All rights reserved

Figure 19. Fabrication procedure using smaller diamond substrates to manufacture a larger mosaic crystal. Schematic drawing courtesy of Excellent Diamond Products, EDP Corporation.[57] <rqy> author: did you ask for permission to use this image?<rqy>

Pending further development in tiling, and with homoepitaxy seemingly stalled at whatever sizes are available as substrates, we also look to heteroepitaxy to provide larger diamond areas, with deposition on silicon wafers as the holy grail of the field.

In a blend of heteroepitaxy and mosaic tiling, a related approach involves an arrangement of cube shaped HPHT diamonds, their orientations aligned by as-grown natural growth faces,[58] as shown in **Figures 20** and **21.**

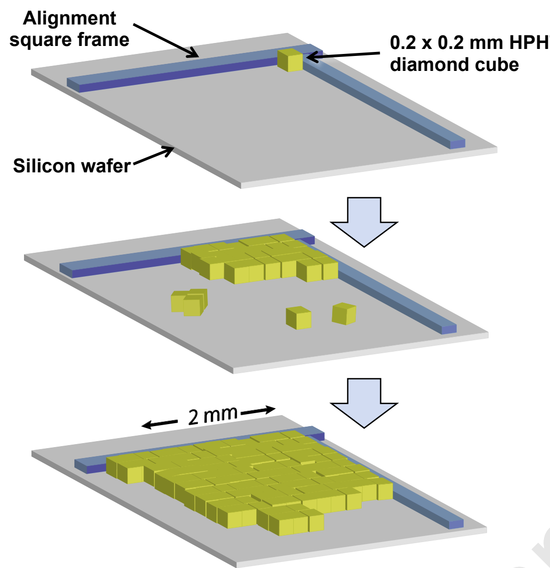

Figure 20. Process to self-align small faceted cubic high-pressure, high-temperature HPHT crystals. After alignment low-pressure homoepitaxial diamond growth is used to cement the crystals together.

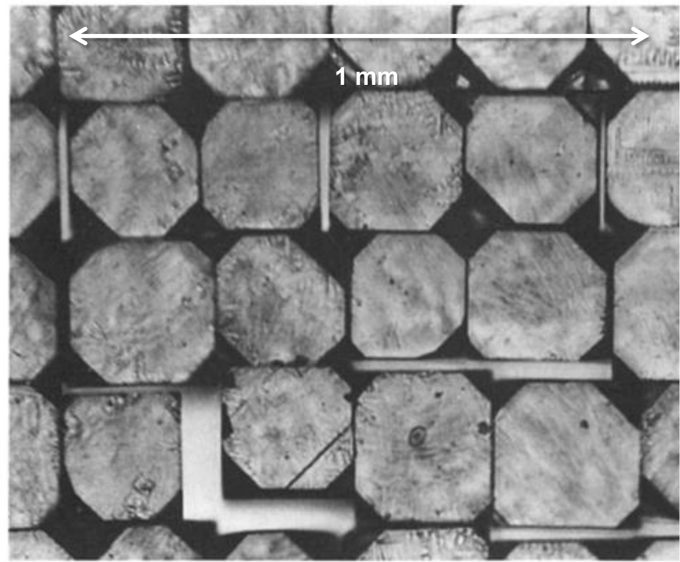

Figure 21. Optical micrograph of self-aligned cubic HPHT crystals just before homoepitaxial growth. The crystal in-plane orientation is ± 1° and the tilt off the axis normal to the substrate is ± 0.5°.[58]

Author Manuscript

If the HPHT diamonds are instead octahedrons, faceted by (111) planes, then alignment is accomplished with anisotropic etch pits faced with (111) planes in (100) Si wafers.[59] Both approaches use the natural facets of the crystals for alignment rather than human/machine precision. Although the approach has only been attempted via hot-filament growth, the approach may yet yield wafer-scale material.

3.4 Heteroepitaxial Diamond Growth Two groups in the 1990's began development of heteroepitaxial growth of diamond on single crystal silicon wafers[60,61] using a process that was developed to enhance random diamond nucleation.[62,63] Both groups used the same procedure with small variations. The starting Si wafer was cleaned and inserted into a diamond growth system having established diamond growth conditions, nominally via a plasma formed in a hydrogen-methane mixture. However, the wafer was DC biased from -100 to -300 volts with bias currents >100 mA. This results in an amorphous carbon layer instead of diamond

This article is protected by copyright. All rights reserved

growth. However, in this carbon layer diamond crystals nucleate heteroepitaxially on the Si crystal.[63] After a nucleation period, the bias voltage is removed and growth conditions for homoepitaxial diamond are established. The amorphous carbon etches away and diamond nuclei expand and merge to yield a continuous diamond film, pictorially shown in **Figure 22.**

In 1996 Ohtsuka demonstrated heteroepitaxial diamond on an Ir film haereroepitaxilly grown on a single crystal MgO substrate.[64] Professor Matthias Schreck, his students, and collaborators have used these previous 1990's developments to deliver the largest single-crystal wafer seen to date.[65] The approach starts with a silicon wafer with an epitaxial layer of yttria-stabilized zirconia, YSZ, chosen as a reasonable lattice-match to diamond. Atop that, iridium, another reasonably good lattice-matched material (within 7%) provides the epitaxial surface, as shown in **Figure 22**. The final material stack, **Figure 23**, is the result of decades of research and experimentation and the precise mechanism of growth is an ongoing topic of research. The 3.6-inch wafer, shown in **Figure 24**, is a remarkable accomplishment given the lattice mismatch with iridium. The resulting diamond substrates are characterized in detail in reference [66].

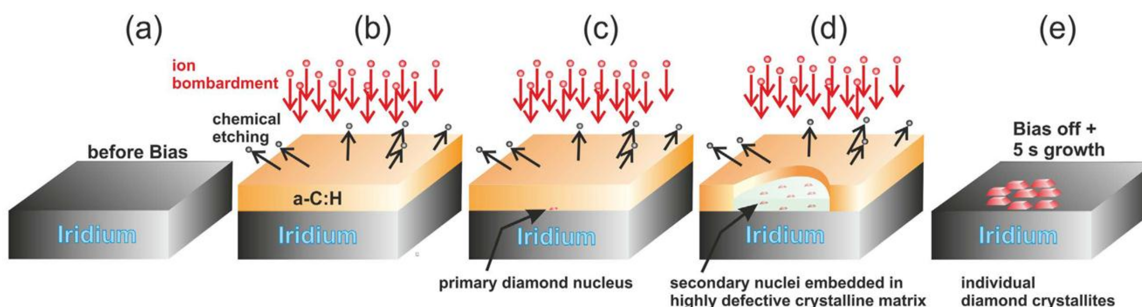

Figure **22. Shows the sequence to generate heteroepitaxial diamond on an Ir layer. (a) No diamond nuclei exist on the Ir in the plasma before biasing. (b-d) When Ir substrate is negatively biased an amorphous layer forms, in which the diamond nuclei form and grow laterally on the Ir surface. (e) When the bias is removed, the amorphous layer is etched away and the nuclei grow together to form a continuous film.** Reproduced under the terms of a Creative Commons Attribution 4.0 International License.[65] Copyright 2017, The Authors, published by Nature Research.

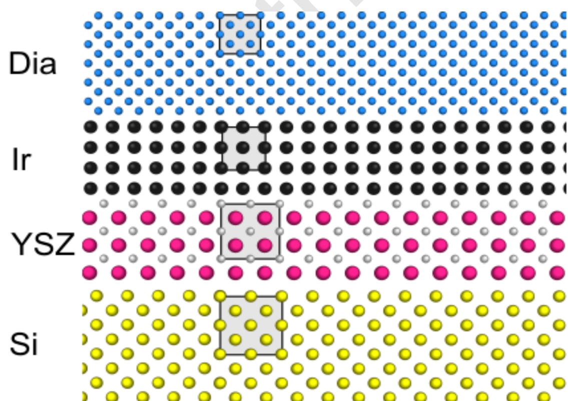

Figure 23. Shows the structure used to grow heteroepitaxial diamond starting with a Si

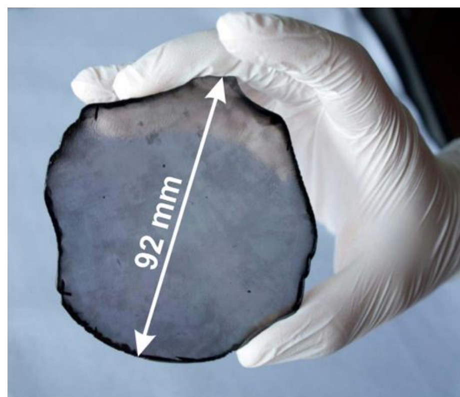

Figure 24. Freestanding 31 g, 3.6-inch-diameter unpolished diamond single-crystal

This article is protected by copyright. All rights reserved

substrate. The yttria-stabilized zirconia (ZrO_2), YSZ, keeps the Ir from reacting with the Si substrate. Figure 24 shows the resulting heteroepitaxial diamond wafer. Reproduced under the terms of a Creative Commons Attribution 4.0 International License.[65] Copyright 2017, The Authors, published by Nature Research.

wafer synthesized by heteroepitaxy on Ir/YSZ/Si(001). Reproduced under the terms of a Creative Commons Attribution 4.0 International License.[65] Copyright 2017, The Authors, published by Nature Research.

Another group has taken on the task of relieving the crystallographic and thermal mismatch between substrate and epitaxial layer with extensive etching of the initial diamond heteroepitaxial layer to produce a wafer of micro-needles upon which further epitaxy is strain-relieved relative to the substrate. An example is shown in **Figure 25**. Similar techniques have been used since the 1980's for the epitaxial growth of GaN and Ge on Si.[67,68]

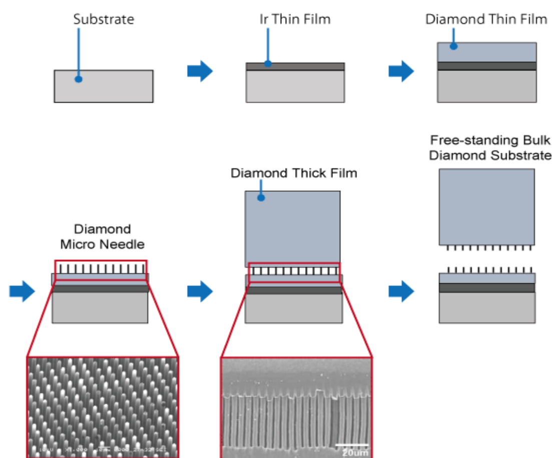

Figure 25. The process for growing heteroepitaxial crystalline diamond, using a procedure to minimize stress from lattice mismatch and differential thermal expansion. Picture courtesy of Adamant Namiki Precision Jewel Co.[69] <qry> author: did you ask for permission to use this image?<qry>

Author Manuscript

4. Conclusions

After significant worldwide research, the promise shown by the semiconductor properties of diamond is beginning to be realized in actual devices. Kawarada reported in 2010 a MISFET on (110) textured polycrystalline diamond substrates with drain currents of 0.8 to 1.2 A mm^{-1} [39,45] and Hirama has reported in 2012 devices also on polycrystalline diamond substrates with drain currents of 1.35 A mm^{-1}.[19] With diamond's thermal conductance and high breakdown voltage, these devices could be competitive with other semiconductor devices. Both of these results have proven difficult to reproduce, though several groups have reported drain currents $\leq$ 0.6 A mm^{-1} [70,71] using air transfer doping which is known to be unstable with temperature and time, an example of which is shown in **Figure 10**. Macdonald,[71] Verona,[72] and Tordjman [73] using transition metal oxides have demonstrated lower resistances, 1.5 to 4 kΩ sq^{-1}, than most Al_2O_3-capped diamond, 4 to 12 kΩ sq^{-1}, [39] but have not yet been able to fabricate MISFETs with drain currents > 0.4 A mm^{-1}. This could be the result of the transition metal oxides changing their valence state under the high electric fields generated in a MISFET, mobile ions in the oxide layer, or just device fabrication issues. WO_3, MoO_3, and V_2O_5 are

This article is protected by copyright. All rights reserved

electrochromic, changing their valence state and color when current is passed through them.[74] Since the gate of a MISFET is the region of highest electrical field through the oxide, a change in the MISFET threshold voltage during operation could be an indication of a change in the valence state of these oxide.

Delta-doped FET models have shown high theoretical RF power levels of ~70 W mm^{-1}.[47] In contrast, after much development, today's state of the art industrial AlGaN/GaN HEMTs mounted on diamond heatsinks are at no higher than 19.9 W mm^{-1},[75] and research devices have been reported with limited operational life and RF power levels of 41 W mm^{-1}.[76] Delta doping requires precise control of the starting diamond substrate, the impurities, and the rapid switching of growth conditions in order to form the necessary atomically sharp boundary layers. Several groups have attempted this and after years of research recent reports have been published of delta-doped material with properties that could make competitive diamond FETs. To our knowledge, no FETs have been fabricated on this material as yet.

In spite of the early maturity stage of the diamond FETs described above, key building blocks and existence proofs have been demonstrated which show the promise of diamond FETs once all the key ingredients can be integrated into single devices. Indeed, all semiconductor-device technologies had to pass through this stage of maturation, including Si, GaAs, and GaN. These device building blocks, coupled with the recent demonstration of ~4-inch single-crystal diamond wafers, opens the door to a diamond power-FET manufacturing capability someday.

Acknowledgments

Distribution Statement: A. Approved for public release - distribution is unlimited.
This material is based upon work supported by the Assistant Secretary of Defense for Research and Engineering under Air Force Contract No. FA8702-15-D-0001. Any opinions, findings, conclusions, or recommendations expressed in this material are those of the author(s) and do not necessarily reflect the views of the Assistant Secretary of Defense for Research and Engineering.

Conflict of Interest

The authors declare no conflict of interest.

Keywords

diamond field effect transistors, diamond heteroepitaxy, atomic layer deposition, NO_2, diamond delta doping.

References

[1] J. Y. Tsao , S. Chowdhury , M. A. Hollis , D. Jena , N. M. Johnson , K. A. Jones , R. J. Kaplar , S. Rajan , C. G. Van de Walle , E. Bellotti , C. L. Chua , R. Collazo , M. E. Coltrin , J. A. Cooper , K. R. Evans , S. Graham , T. A. Grotjohn , E. R. Heller , M. Higashiwaki , M. S. Islam , P. W. Juodawlkis , M. A. Khan , A. D. Koehler , J. H. Leach , U. K. Mishra , R. J. Nemanich , R. C. N. Pilawa-Podgurski , J. B. Shealy , Z. Sitar , M. J. Tadjer , A. F. Witulski , M. Wraback , J. A. Simmons, Adv. Electron. Mater. **2018**, 4, 1600501.

[2] A. Huang, IEEE Elect. Dev. Lett. **2004,** 25, 298.

[3] B. J. Baliga, IEEE Elect. Dev. Lett. **1989,** 10, 455.

[4] E. O. Johnson, RCA Rev. **1965,** 26, 163.

[5] Semiconductors on NSM; http://www.ioffe.ru/SVA/NSM/Semicond/Diamond/bandstr.html#Donors

This article is protected by copyright. All rights reserved

Author Manuscript

[6] A.T. Collins, E. C. Lightowlers, Electrical Properties in The Properties of Diamond, Vol. 3 (Ed. J. E. Field 1979), Academic Press, London **1979**, 81.
[7] M. Werner, R. Job, A. Zaitzev, W. R. Fahrner, W. Seifert, C. Johnston, P. R. Chalker, Phys. Stat. Sol. (A) **1996**, 154, 385.
[8] M. Riedel, J. Ristein, L. Ley, Diam. Relat. Mater. **2004**, 13, 746.
[9] F. Maier, M. Riedel, B. Mantel, J. Ristein, L. Ley, Phys. Rev. Lett. **2000,** 85, 3472.
[10] R. Sung Gi, T. Ishikawa, S. Tanaka, T. Kimura, Y. Akiba, M. Iida, Jpn. J. Appl. Phys. **1997**, 36, 2057.
[11] H. Sato, M. Kasu, Diam. Relat. Mater., **2012**, 24, 99.
[12] M.W. Geis, T.H. Fedynyshyn, M.E. Plaut, T.C. Wade, C.H. Wuorio, S.A. Vitale, J.O. Varghese, T.A. Grotjohn, R.J. Nemanich, M.A. Hollis, Diam. Relat. Mater. **2018**, 84, 86094.
[13] T. C. Wade, M.W. Geis, T.H. Fedynyshyn, S.A. Vitale, J.O. Varghese, D.M. Lennon, T.A. Grotjohn, R.J. Nemanich, M.A. Hollis, Diam. Relat. Mater. **2017,** 76,79–85.
[14] D. Kueck, S. Jooss, E. Kohn, Diam. Relat. Mater. **2009** 18, 1306–1309.
[15] A. Hiraiwa, A. Daicho, S. Kurihara, Y. Yokoyama, H. Kawarada, J. Appl. Phys. **2012**, 112, 124504.
[16] S.A.O. Russell, L. Cao, D. Qi, A. Tallaire, K.G. Crawford, A.T.S. Wee, D.A.J. Moran, Appl. Phys. Lett. **2013**, 103; 202112.
[17] M. Tordjman, C. Saguy, A. Bolker, R. Kalish, Adv. Mater. Interfaces **2014**, 1, 1300155.
[18] K.G. Crawford, L. Cao, D. Qi, A. Tallaire, E. Limiti, C. Verona, A.T.S. Wee, D.A.J. Moran, Appl. Phys. Lett. **2016**, 108, 042103.
[19] K. Hirama, H. Sato, Y. Harada, H. Yamamoto, M. Kasu, Jpn. J. Appl. Phys. **2012**, 51, 090112.
[20] S. Sato, K. Tsuge, T. Tsuno, T. Ono, H. Kawarada, Int. Conf. Solid State Devices and Materials (SSDM) **2010**, 908.
[21] H. Kawarada, T. Yamada, D. Xu, H. Tsuboi, T. Saito, A. Hiraiwa, Electron Device Meeting (IEDM), IEEE Int., **2014**, 11.2.1-4.
[22] M. Syamsul, Y. Kitabayashi, D. Matsumura, T. Saito, Y. Shintani, H. Kawarada, Appl. Phys. Lett. **2016**, 109, 203504.
[23] X. Yu, J. Zhou, C. Qi, Z. Cao, Y. Kong, T. Chen; IEEE Electr. Dev. Lett. 39 (2018) 1373-1376.
[24] V. Camarchia, F. Cappelluti, G. Ghione, E. Limiti, D. A. J. Moran, M. Pirola, Proc. Int. Workshop Integr. Nonlinear Micro. Millimetre-Wave Circuits (INMMiC), Apr. **2014**; doi:10.1109/INMMIC.2014.6815102
[25] K. Ueda, M. Kasu, Y. Yamauchi, T. Makimoto, M. Schwitters, D. J. Twitchen, G. A. Scarsbrook, S. E. Coe, IEEE Elect. Dev. Lett. **2006**, 27, 570.
[26] A. Fiori, J. Pernot, E. Gheeraert, E. Bustarret, Phys. Status Solidi A **2010,** 2072084–2087; DOI 10.1002/pssa.201000062
[27] G. Chicot, A. Fiori, P. N. Volpe, T. N. Tran Thi, J. C. Gerbedoen, J. Bousquet, M. P. Alegre, J. C. Piñero, D. Araújo, F. Jomard, A. Soltani, J. C. De Jaeger, J. Morse, J. Härtwig, N. Tranchant, C. Mer-Calfati, J. C. Arnault, J. Delahaye, T. Grenet, D. Eon, F. Omnès, J. Pernot, E. Bustarret, J. Appl. Phys. **2014**, 116,083702.
[28] J. E. Butler, A. Vikharev, A Gorbachev, M. Lobaev, A. Muchnikov, D. Radischev, V. Isaev, V. Chernov, S. Bogdanov, M. Drozdov, E. Demidov, E. Surovegina, V. Shashkin, A. Davdov, H. Tan, L. Meshi, A. C. Pakpour-Tabrizi, M.-L. Hicks, R. B. Jackman, Phys. Status Solidi **2017**, 11, 1600329.
[29] R. S. Balmer, I. Friel, S. Hepplestone, J. Isberg, M. J. Uren, M. L.Markham, N. L. Palmer, J. Pilkington, P. Hugget, S.Majdi, R. Lang, J. Appl. Phys. **2013**, 113, 033702.
[30] G. Chicot, T. N. Tran Thi, A. Fiori, F. Jornard, E. Gheeraert, E. Bustarret, and J. Pernot, Appl. Phys. Lett. **2012** 101, 162101.
[31] H. El-Hajj, A .Denisenko, A. Kaiser, R. S. Balmer, E. Kohn, Diam. Relat. Mater. **2008**, 17, 1259.
[32] R. Edgington, S. Sato, Y. Ishiyama, R. Morris, R. B. Jackman, H. Kawarada, J Appl. Phys. **2012**, 111, 033710.
[33] H. Sato, M. Kasu, Diam. Relat. Mater. **2013**, 31, 47
[34] Y. Takagi, K. Shiraishi, M. Kasu, H. Sato, Surf. Sci. **2013**, 609, 203.
[35] P. Rivero, W. Shelton, V. Meunier, Carbon **2016**, 110, 469.
[36] S. Brunauer, P. H. Emmett, E. Teller, J. Am. Chem. Soc. **1938**, 60, 309.
[37] M. Riedel, J. Ristein, L. Ley, Phys. Rev. B **2004**, 69, 125338.
[38] L. Reggiani, D. Waechter, S. Zukotynski, Phys. Rev. B **1983**, 28, 3550–3554
[39] K. Hirama, H. Takayanagi, S. Yamauchi, J. H. Yang, H. Kawarada, H. Umezawa, Appl. Phys. Lett. **2008,** 92, 112107.
[40] Z. He, C. Zhong, S. Su, M. Xu, H. Wu, Y. Cao, Nature Photonics **2012**, 6, 591.

Author Manuscript

This article is protected by copyright. All rights reserved

[41] C. Verona, W. Ciccognani, S. Colangeli, E. Limiti, M. Marinelli, G. Verona-Rinati, J. Appl. Phys. **2016,** 120, 025104.
[42] F. Maier, J. Ristein, and L. Ley, Phys. **2018**, 112, 181602.
[44] K. G. Crawford, D. Qi, J. McGlynn, T. G. Ivanov, P. B. Shah, J. Weil, A. Tallaire, A. Y. Ganin, D. A. J. Moran, , Sci. Rep. **2018**, 8, 3342.
[45] H. Kawarada, Jpn. J. Appl. Phys. **2012,** 51, 090111.
[46] Y. Yang, F. A. Koeck, M. Dutta, X. Wang, S. Chowdhury, R. J. Nemanich, J. Appl. Phys. **2017**, 122, 155304.
[47] A. DenisenkoT, E. Kohn, Diamond & Related Materials 14 (2005) 491–498
[48] J. Scharpf, A. Denisenko, C. I. Pakes, S. Rubanov, A. Bergmaier, G. Dollinger, C. Pietzka, E. Kohn, Phys. Status Solidi A **2013,** 210, 2028–2034.
[49] M.A.Lobaev, A.M.Gorbachev, A.L.Vikharev, V.A.Isaev, D.B.Radishev, S.A.Bogdanov, M.N.Drozdov, P.A.Yunin, J.E.Butler, Thin Solid Films **2018**, 653, 215.
[50] H. Sato, M. Kasu, Diam. Relat. Mater. 31 (Rev. B **2001**, 64, 165411.
[43] C. Verona, F. Arciprete, M. Foffi, E. Limiti, M. Marinelli, E. Placidi, G. Prestopino, G. V. Rinati, Appl. Phys. Lett. 2013) 47–49.
[51] Neocoat SA. https://www.neocoat.ch/en/technology/cvd-technologies
[52] F.X. Lu_, W.Z. Tang, T.B. Huang, J.M. Liu, J.H. Song, W.X. Yu, Y.M. Tong, Diam. Relat. Mater. **2001**, 10, 1551.
[53] J. E. Butler, R. L. Woodin,. Phil. Trans. R. Soc. A **1993**, 342, 209.
[54] D. G. Goodwin, J. E. Butler, in: M. A. Prelas, G. Popovici, L. K. Biglow (Eds.) Handbook of Industrial Diamonds and Diamond Films, Marcel Dekker, Inc., NY, NY, **1997**, 527.
[55] Y.Mokuno, A Chayahara, Y. Soda, H. Yamada, Y. Horino, N. Fujimori, Diam. Relat. Mater. **2006**, 15, 455.
[56] T. Straubingr, R. Eckstein, M. Vogel, A. Weber, SiC Bulk Crystal Growth, presented at 7th International workshop on Crystal Growth Technology, Potsdam, **2017**.
[57] Excellent Diamond Products, EDP, Corporation http://www.d-edp.jp/en/
[58] M.W. Geis, N.N. Efremow, R. Susalka, J.C. Twichell, K.A. Snail, C. Spiro, B. Sweeting, S. Holly, Diam. Relat. Mater. **1994**, 4, 76.
[59] M. W. Geis, Diam. Relat. Mater. **1992**, 1, 684.
[60] S. D. Wolter, B. R. Stoner, J. T. Glass, P. J. Ellis, D. S. Buhaenko, C. E. Jenkins, P. Southworth, Appl. Phys. Lett. **1993**, 62, 1215.
[61] X. Jiang, C.-P. Klages, R. Zachai, M. Hartweg, H.-J. Füsser, Appl. Phys. Lett. **1993**, 62, 3438.
[62] S. Yugo, T. Kanai, T. Kimura, T. Muto, Appl. Phys. Lett. **1991**, 58, 1036.
[63] B.R. Stoner, G. -H. M. Ma, S. D. Wolter, J. T. Glass, Phys. Rev. B **1992**, 45, 11067.
[64] K. Ohtsuka, K. Suzuki, A. Sawabe, T. Inuzuka, Jpn. J. Appl. Phys. 35 (1996) L1072-L1074
[65] M. Schreck, S. Gsell, R. Brescia, M. Fischer, Sci. Rep. **2017**, 7, 44462.
[66] B.-C. Gallheber, M. Fischer, M. Mayr, J. Straub, M. Schreck, J. Appl. Phys. **2018**, 123, 225302.
[67] S. Luryi, E. Suhir, Appl. Phys. Lett. **1986,** 49, 140.
[68] S. D. Hersee, X. Y. Sun, X. Wang, M. N. Fairchild, J. Liang, J. Xu, J. Appl. Phys. **2005**, 97, 124308.
[69] Adamant Namiki Precision Jewel Co., https://www.ad-na.com/en/product/jewel/material/diamond.html
[70] J. Weil, P. Shah, A. G. Birdwell, T. Ivanov, GOMACTech **2018**
[71] D. A. Macdonald, K. G. Crawford, A. Tallaire, R. Issaoui, D. A.J. Moran, IEEE Electr. Dev. Lett. EDL **2018**, 061040.
[72] C. Verona, W. Ciccognani, S. Colangeli, E. Limiti, M. Marinelli, G. Verona-Rinati, D. Cannatà, M. Benetti, F. Di Pietrantonio, IEEE Trans. Electr. Dev. **2016**, 63, 4647.
[73] M. Tordjman, K. Weinfeld, R. Kalish, Appl. Phys. Lett., **2017**, 111, 1.
[74] Handbook of Inorganic Electrochromic Materials, ed C. G. Granqvist, Elsevier second impression **2002**.
[75] “www.microwavejournal.com/articles/30880-fujitsu-successfully-triples-output-power-of-gan-transistors” [Online].
[76] Y.-F. Wu, M. Moore, A. Saxler, T. Wisleder, P. Parikh, 2006 64th Device Research Conference 26-28 June 2007, Proceedings **2007,** 151.

Author Manuscript

This article is protected by copyright. All rights reserved

Michael Geis is in the RF Technology Group at Lincoln Laboratory. He received his B.A. in Physics and M.S. in Electrical Engineering from Rice University in 1970. The Ph.D. degree in Space Physics and Astronomy was received also from Rice University in 1976. He worked as a postdoctoral student in the Chemistry Department of Rice University. In 1978, he joined Lincoln Laboratory, Massachusetts Institute of Technology. He developed semiconductor-on-insulator technology using zone-melting-recrystallization, submicrometer structure fabrication and dry etching. More recently he has worked in diamond semiconductor technology, vacuum cathodes, optical limiters, and chemical concentrators for toxic gas detection.

Author Manuscript

This article is protected by copyright. All rights reserved

TOC text

Diamond's properties (highest thermal conductivity, high hole & electron mobilities, & high electric breakdown field) predict that diamond field-effect transistors (FETs) would have superior high-power high-frequency performance over FETs formed in other semiconductors. However, still some technical issues exist for FETs and diamond substrates. This article reviews the state of the art for FET and substrate development.

<qry> Author: Please note that it is not appropriate to use images that are taken from preexisting or already-published sources as part of the TOC image. All parts must be new. If required, please revise your ToC image and provide the revised version by upload with your proof corrections </qry>

Author Manuscript

This article is protected by copyright. All rights reserved